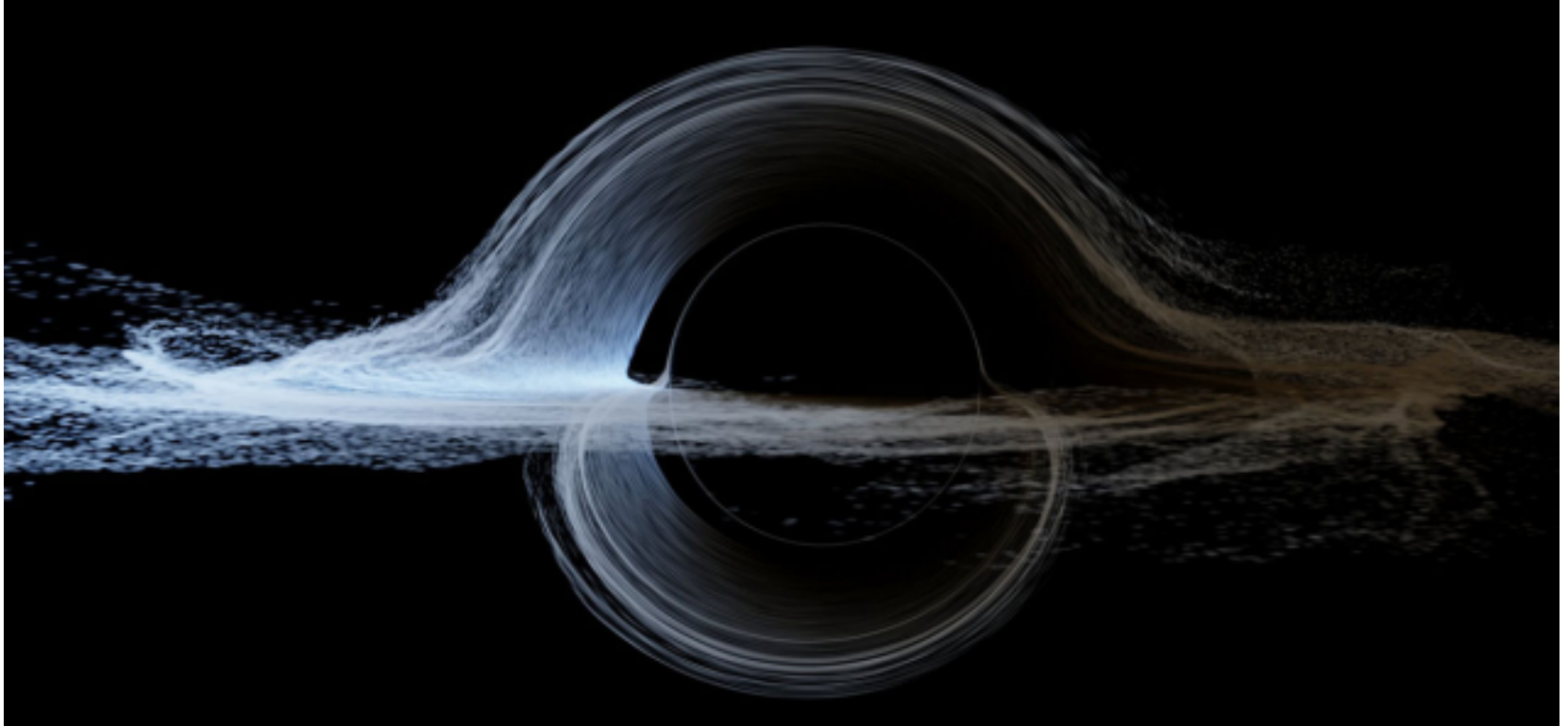


The g -Distribution Method for Measuring the Innermost Stable Circular Orbit



Interstellar: Kip Thorne and Double Negative visual-effects team

Presented by: George Chartas

Manhattan Microlensing 2017

COLLEGE of
CHARLESTON

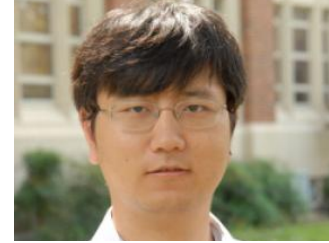
Part 1 in collaboration with:



Chris Kochanek (OSU)



Henric Krawczynski (WUSTL)



Xinyu Dai (OU)



Ana Mosquera (USNA)



Christopher Morgan (USNA)



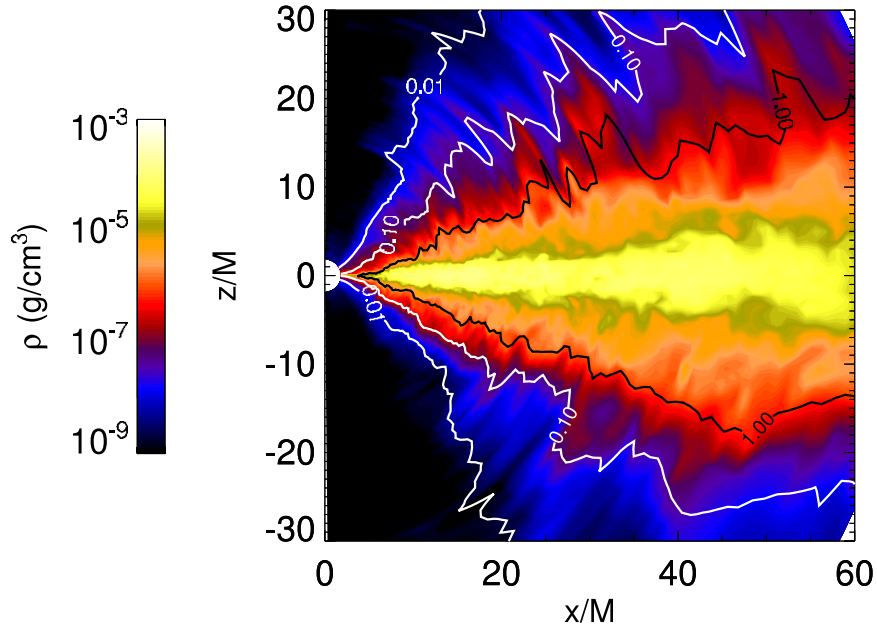
Lukas Zalesky (CofC)

Outline

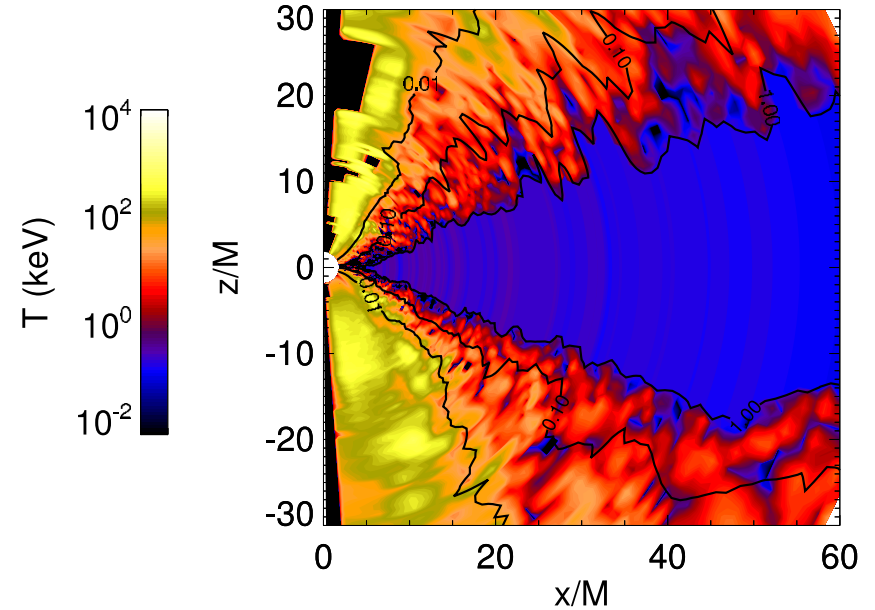
- Accretion Flows and Coronae
- Microlensing used for indirect mapping of disk
- Constraints on Corona Size
- Monitoring of Lensed Quasars
- Constraints on inclination, ISCO, and spin
- Conclusions

Numerical Simulations of Accretion Flows

GRMHD simulations for $M_{\text{BH}} = 10M_{\odot}$, $L=0.1L_{\text{Edd}} = 0.1$, Schnittman+2013

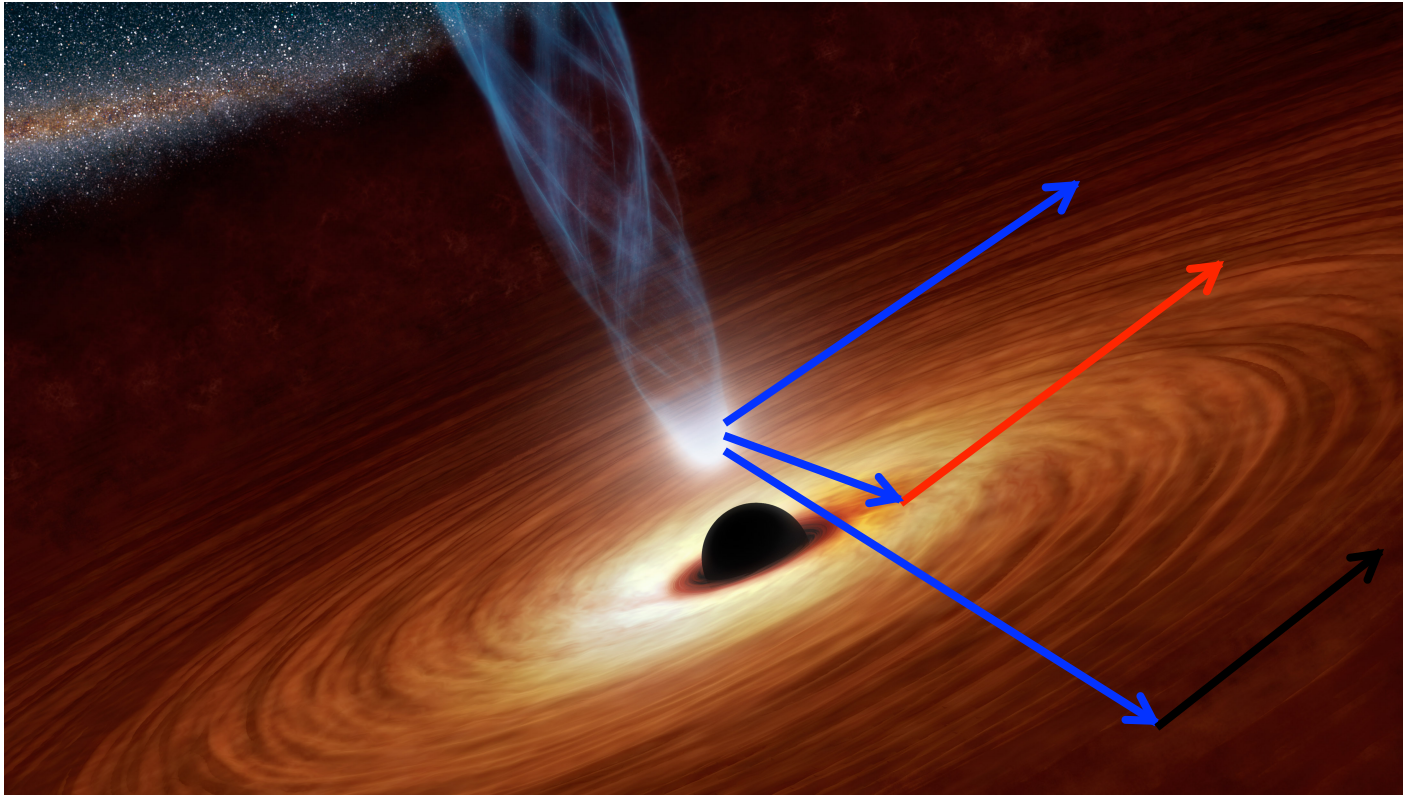


Fluid density profile



Electron temperature in the Corona

Fiducial Model



X-ray Power-Law
from compact corona

Relativistically
Blurred Reflection
(line + continuum)

Distant Reflection
(line + continuum)

Geometrically thin, optically thick accretion
disk emitting primarily in UV/Optical

Quasar Accretion Disk Tomography

Direct imaging of quasars is not possible due to their large distances. Microlensing, however, can resolve:

Structure of AGN Accretion Disks

- The sizes of the Optical and UV regions of AGN
- Comparison with Thin Disk Theory
- Use the distribution of shifts of the Fe line to infer the ISCO, *spin*, and *inclination angle of disk*

Structure of AGN Coronae

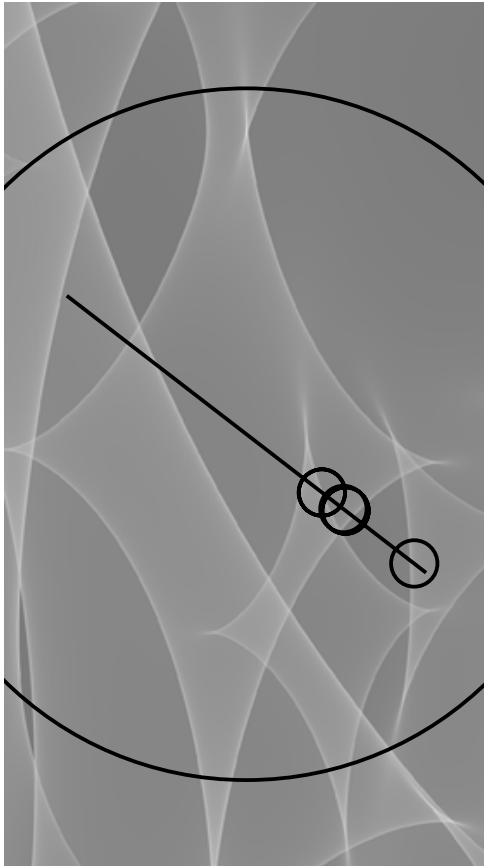
- The sizes of X-ray emitting coronae of AGN

Quasar Accretion Disk Tomography

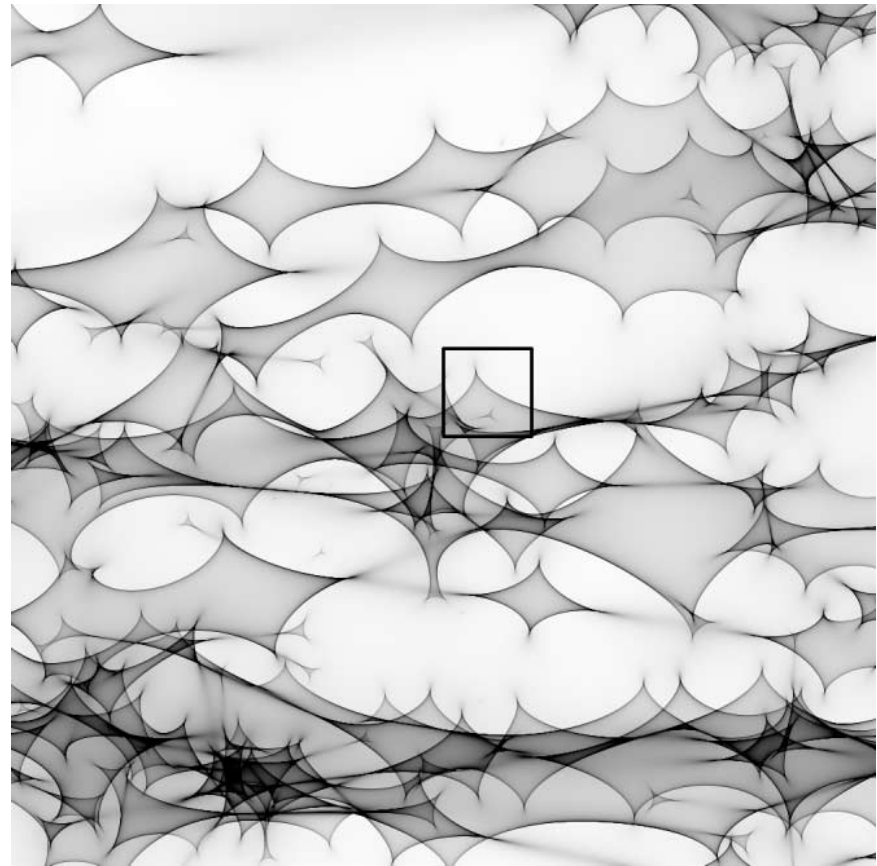
Microlensing Model

- The main free parameters of a microlensing model are:
 - the **sizes** of the emission regions,
 - the mass of the stars doing the **microlensing**,
 - the fraction of normal matter to dark matter in the galaxy doing the lensing
 - the **velocity** describing the motion of the AGN regions across the microlensing caustics.

- The microlensing analysis includes the creation of **many random realizations of the star fields** near each image and the generation of magnification maps.



Simulated magnification map of image B of RXJ 1131 (Dai et al. 2010)



Microlensing map of QSO 2237+0305A image

Dissecting an Accretion Disk with Microlensing

- We are performing multiwavelength monitoring of several quasars :

RX J1131-1231 ($z_s = 0.658, z_l = 0.295$)

Q J0158-4325 ($z_s = 1.29, z_l = 0.317$)

SDSS0924+0219 ($z_s = 1.524, z_l = 0.39$)

Q 2237+030 ($z_s = 1.60, z_l = 0.04$)

HE 0435-1223 ($z_s = 1.689, z_l = 0.46$)

PG 1115+080 ($z_s = 1.72, z_l = 0.31$)

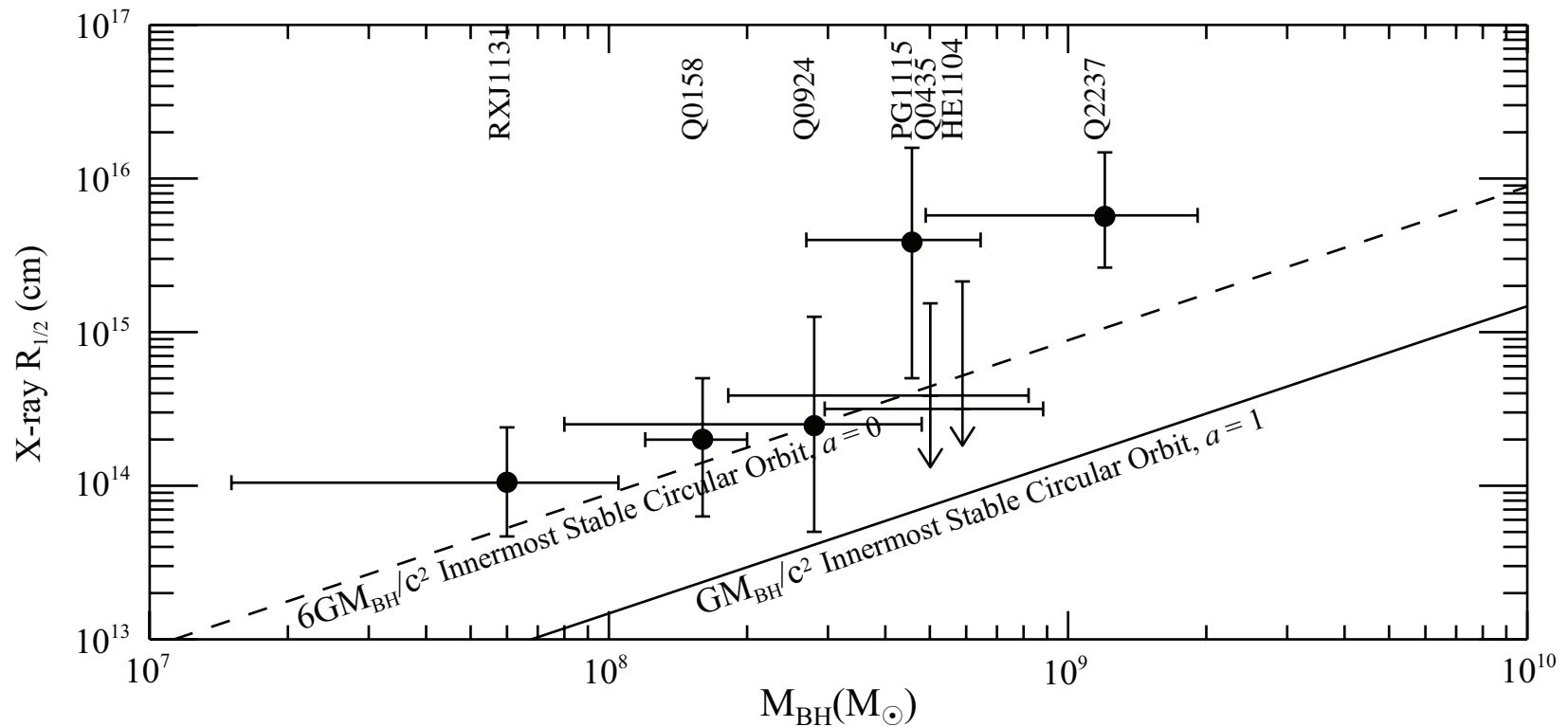
SDSS1004+4112 ($z_s = 1.734, z_l = 0.68$)

QSO 1104-1805 ($z_s = 2.32, z_l = 0.73$)

with the main scientific goal of measuring the emission structure near the black holes in the optical\UV and X-ray bands in order to test accretion disk models.

- X-ray monitoring observations were performed with *Chandra*
- Optical (*B, R* and *I* band) observations were made with the SMARTS Consortium 1.3m telescope in Chile.

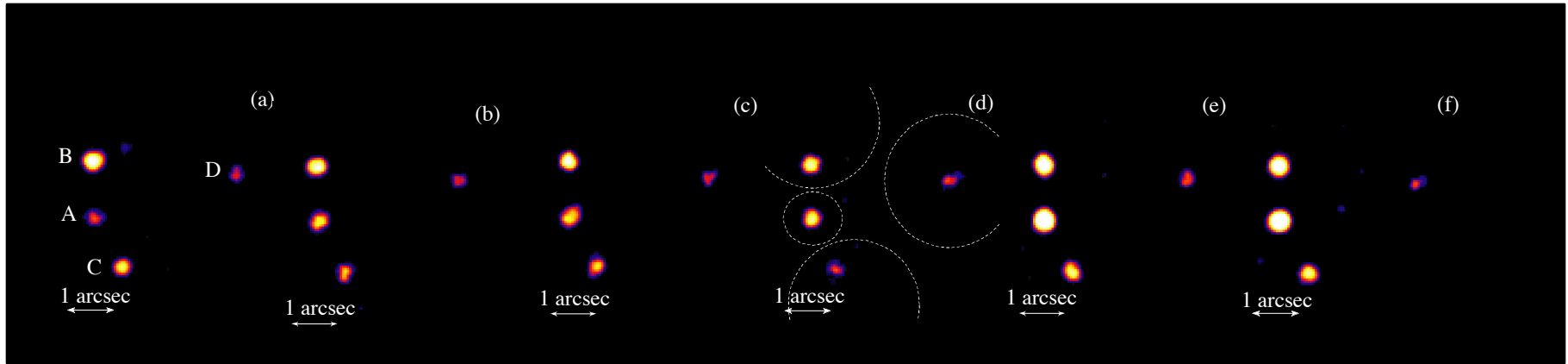
Constraints on Corona Size from Microlensing



X-ray half-light radii of quasars as determined from our microlensing analysis versus their black hole masses.

Chartas+2016

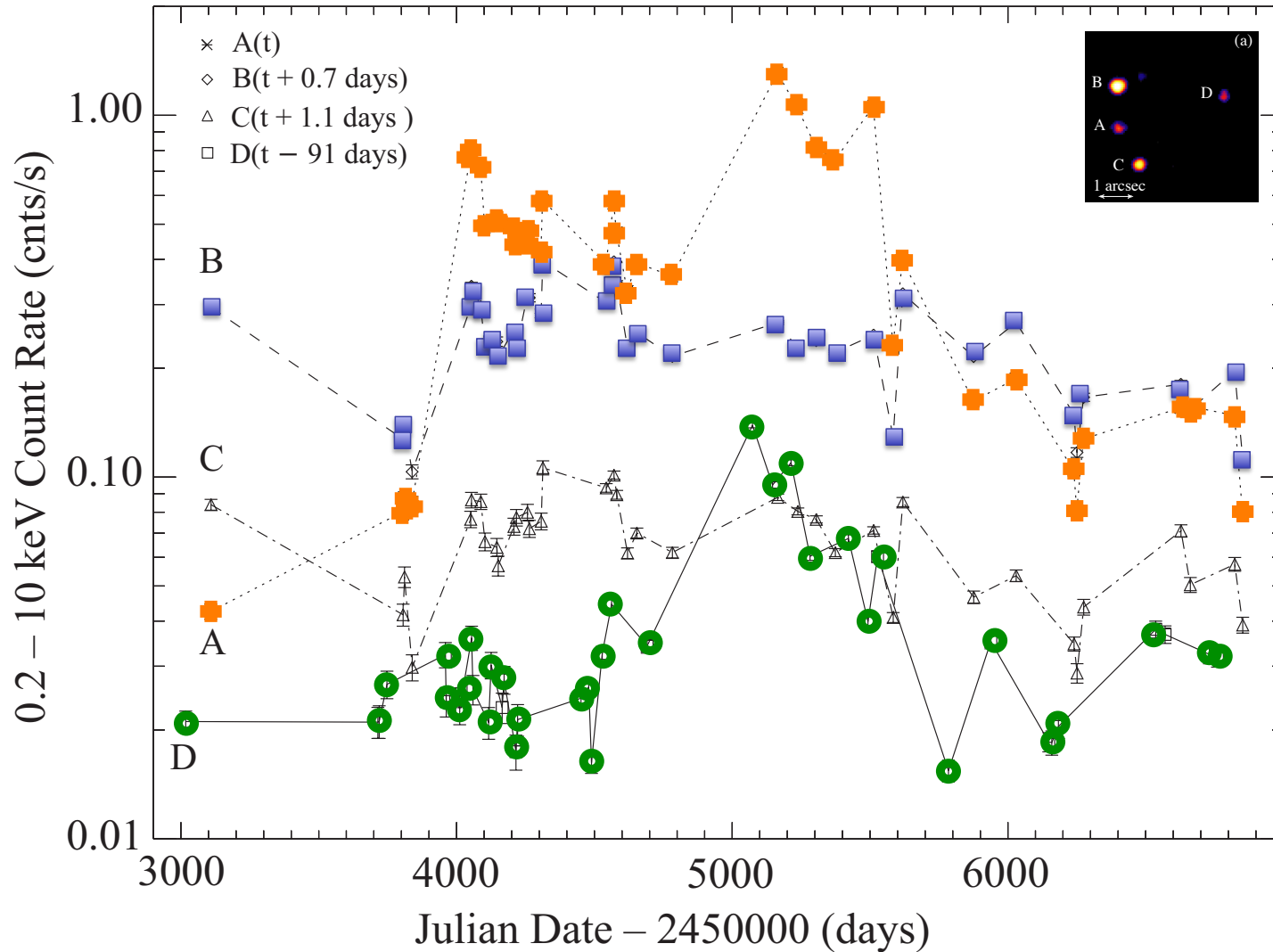
Monitoring of RX J1131-1231 with Chandra



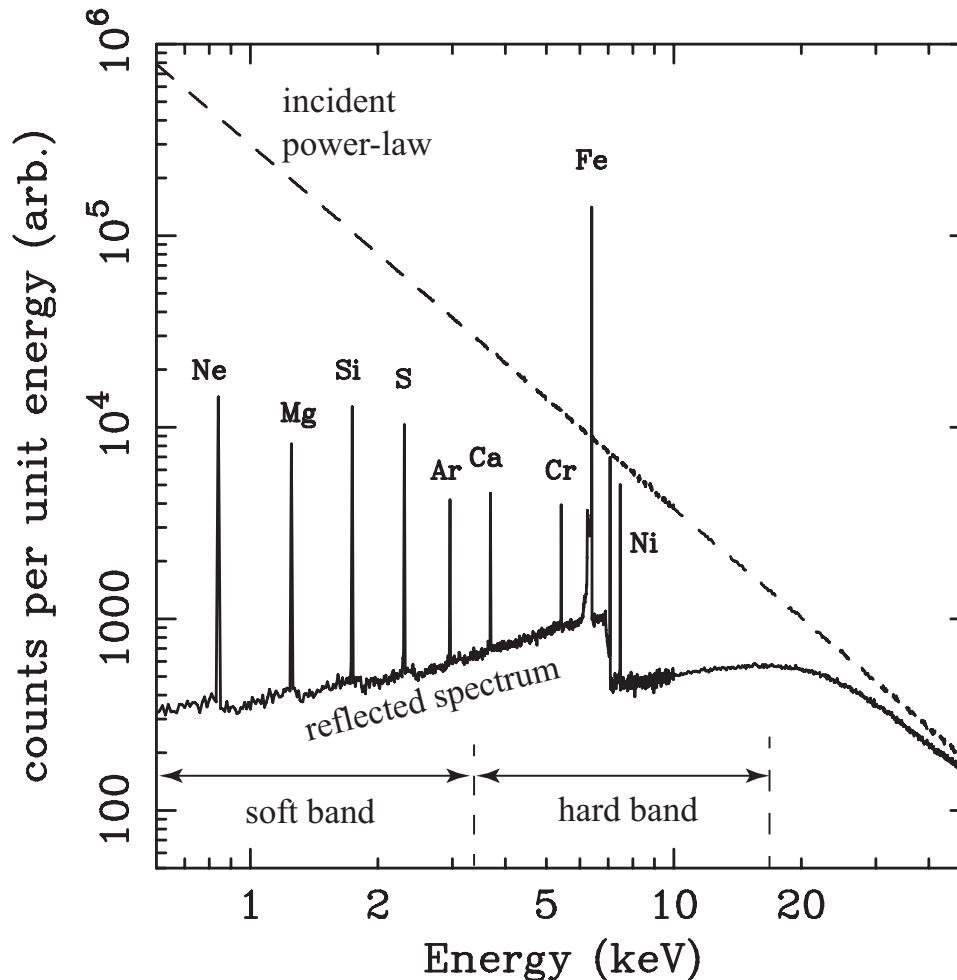
Images in the 0.2 - 10 keV bandpass of the *Chandra* observations of RX J1131-1231.

Data taken between April 4, 2004 & July 1, 2014.
38 pointings, between 4-28 ksec each.

Microensing detected in 0.2 – 10 keV light-curves of RXJ1131

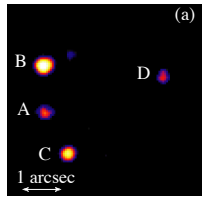


Microensing of a Quasar's Accretion Disk



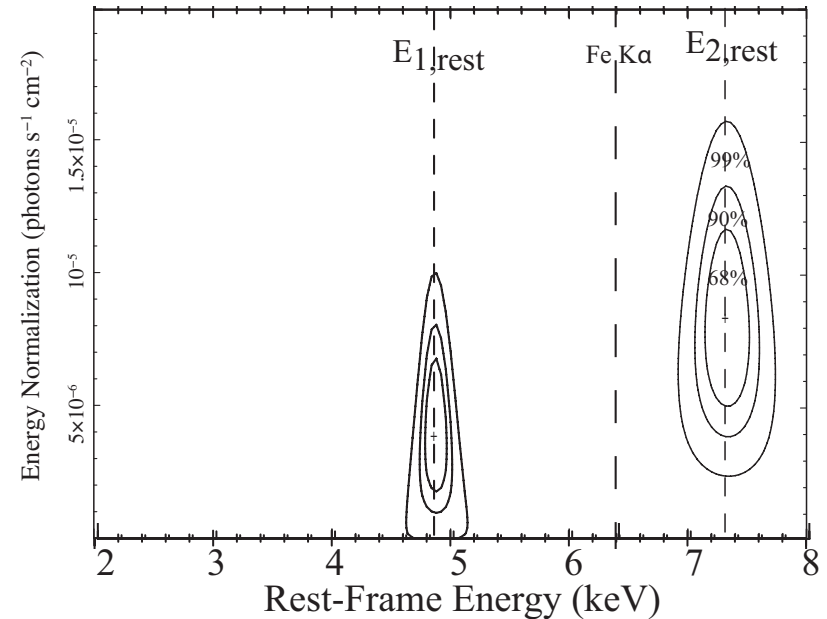
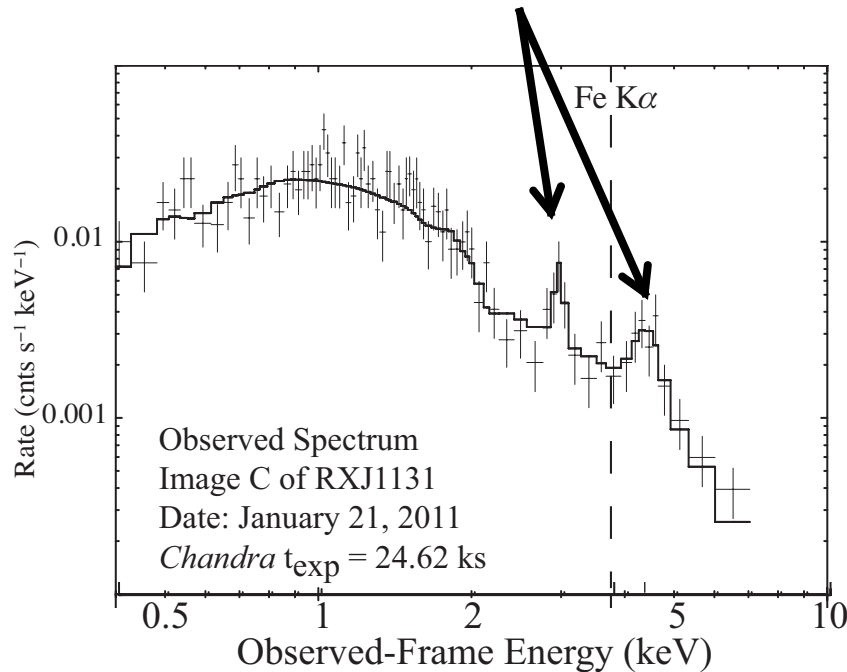
“Reflection” of an incident power-law X-ray spectrum (dashed line) by a cold slab of gas with cosmic abundances. The principal observables from the reflection are the iron K fluorescent line at 6.40keV and a “Compton reflection hump” peaking at ~ 30 keV. Courtesy of Chris Reynolds.

Evidence for Microlensing in all Images of RXJ1131



Shifted Fe K α line in Spectrum of image C (1/21/2011)

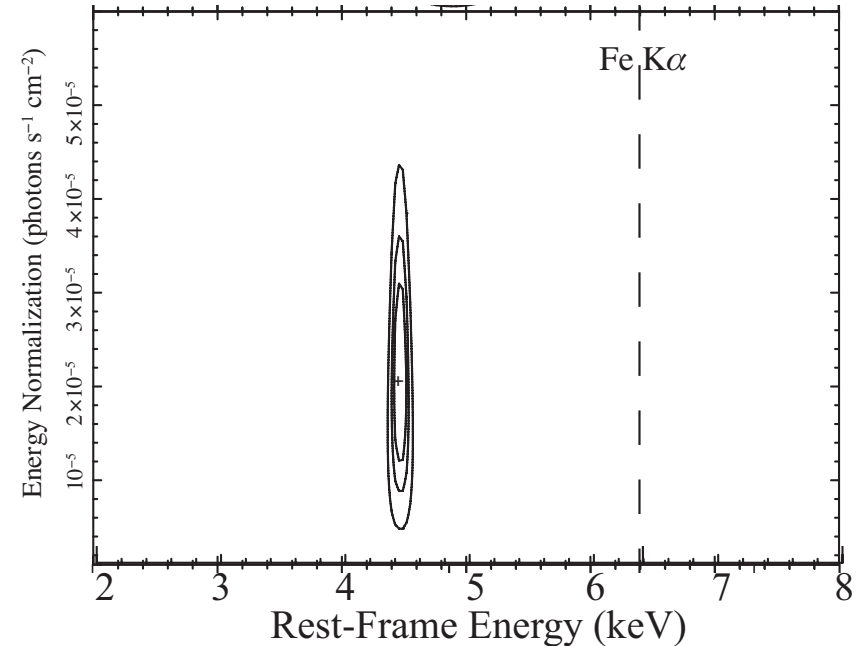
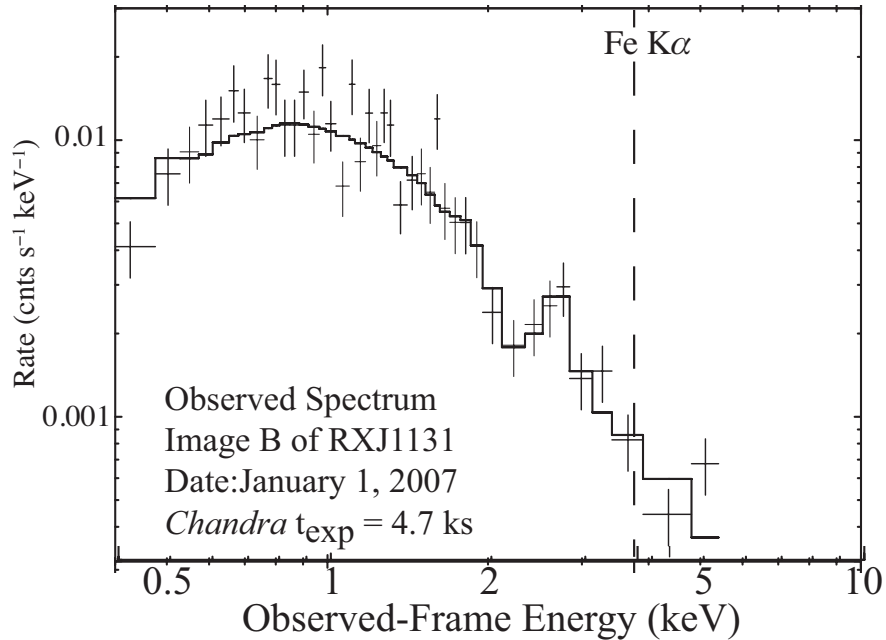
“Double”



- 4 images \times 38 pointings = 152 spectra
- 78 lines ($>90\%$ CL), 21 lines ($>99\%$ CL)

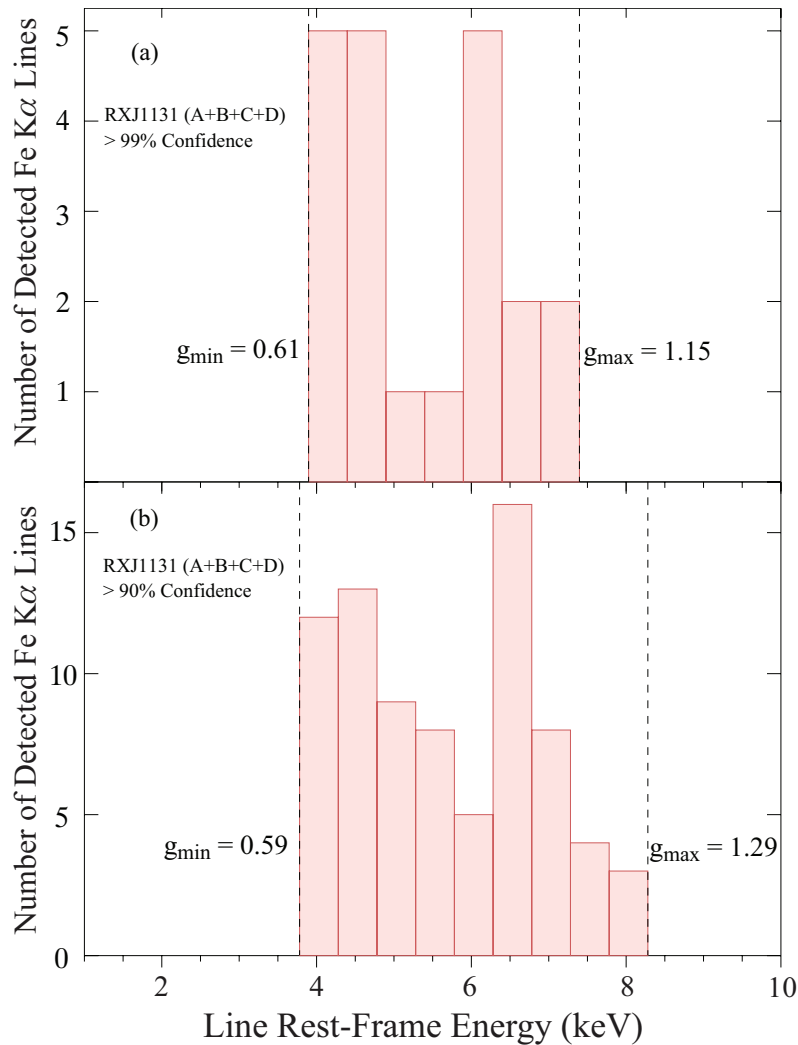
Evidence for Microlensing in all Images of RXJ1131

Shifted Fe K α line in Spectrum of image B (1/1/2007)



Significant spectral variability, including the centroid and equivalent width of the Fe K α line

g-Distribution of Line Centroids of RXJ1131

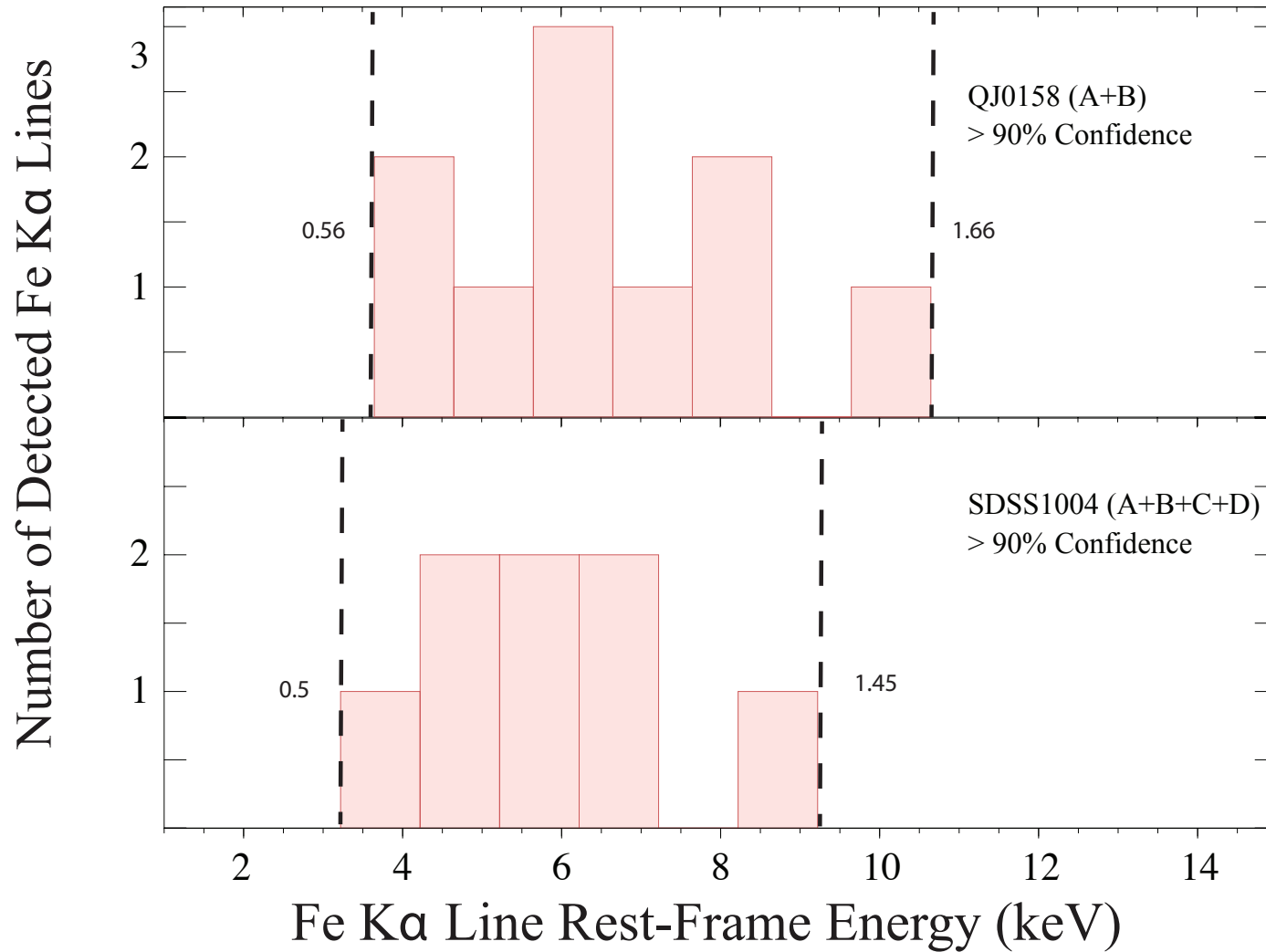


Red/blueshift: 0.61-1.15 (99% CL)

Red/blueshift: 0.59-1.29 (90% CL)

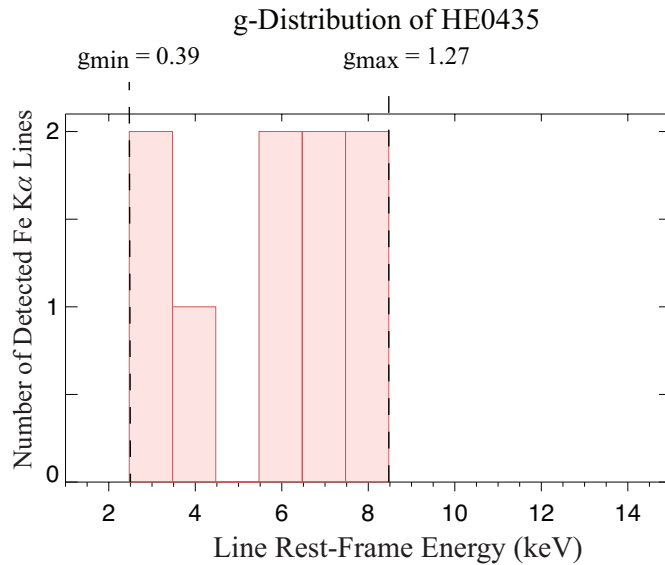
Chartas et al. 2017

g-Distributions of QJ0158 and SDSS1004



Chartas et al. 2017

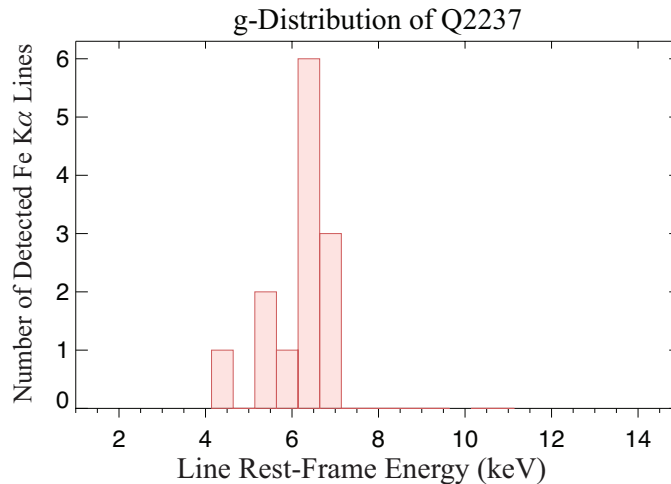
g-Distributions of HE 0435 and Q 2237



HE 0435-1223 ($z_s = 1.689$, $z_l = 0.46$)

Extremal shifts of the Fe K α line energy in HE 0435 imply

- $3r_g < r_{\text{ISCO}} < 4r_g$
- spin ~ 0.7



Q 2237+030 ($z_s = 1.60$, $z_l = 0.04$)

$g_{\max} \sim 7$ keV implies face on geometry

Generalized Doppler Shift

The observed energy of a photon emitted near the event horizon of supermassive black hole will be shifted with respect to the emitted rest-frame energy due to general relativistic and Doppler effects.

$$g = \frac{E_{obs}}{E_{emit}} = \delta \sqrt{\frac{\Sigma \Delta}{A}}$$

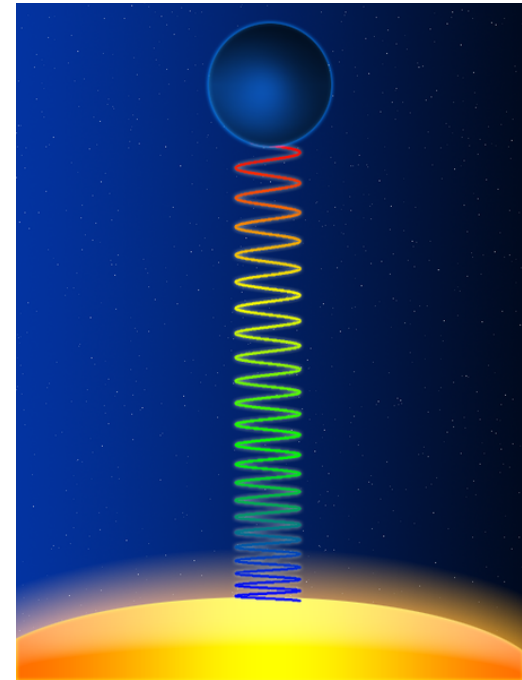
Where the Doppler shift is:

$$\delta = \frac{\sqrt{1 - v_\phi^2}}{1 - v_\phi \cos \theta_c}, \text{ where } v_\phi \text{ is the azimuthal velocity}$$

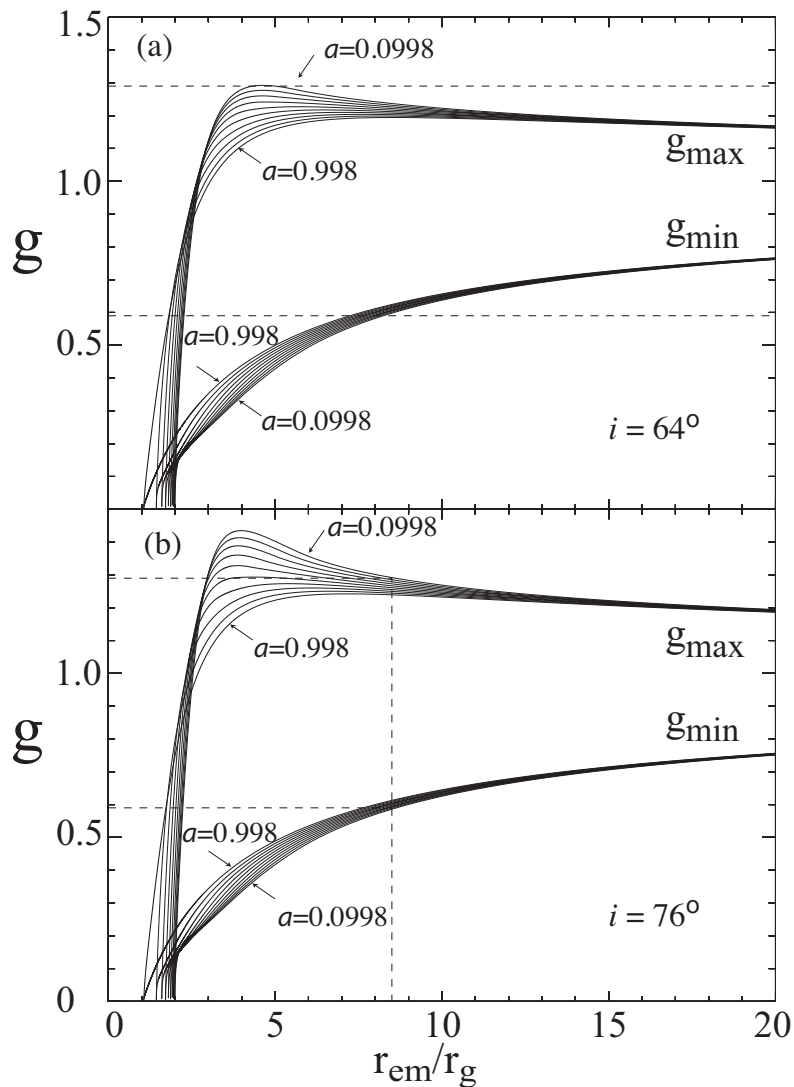
and θ_c is the angle between our line-of-sight and the direction of motion of the emitting plasma.

A , Σ , and Δ are defined as

$$A = (r^2 + a^2)^2 - a^2 \Delta \sin^2 \theta, \quad \Sigma = r^2 + a^2 \sin^2 \theta, \quad \Delta = r^2 - 2r_g r + a^2$$



g versus radius for RXJ1131



$$g_{\max} = 1.29 \rightarrow$$

$$i > 64^\circ$$

$$g_{\max} = 1.29 \rightarrow$$

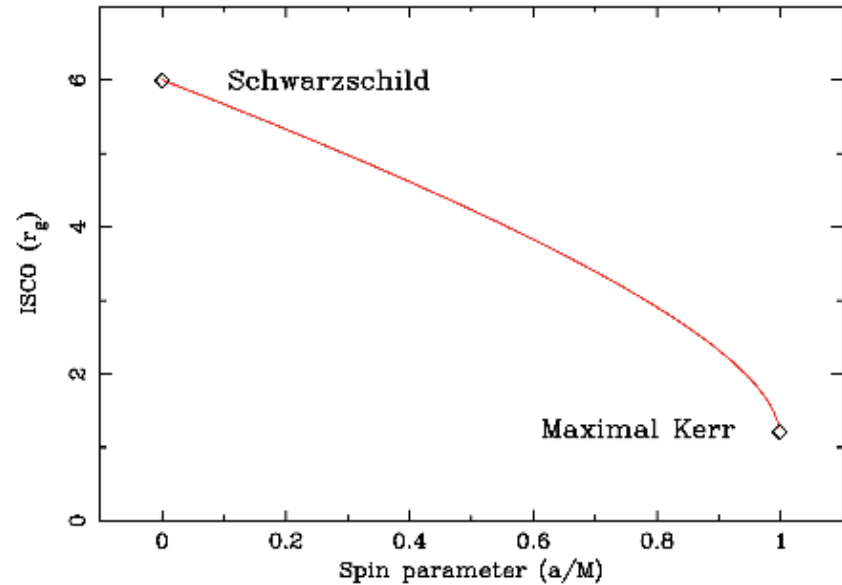
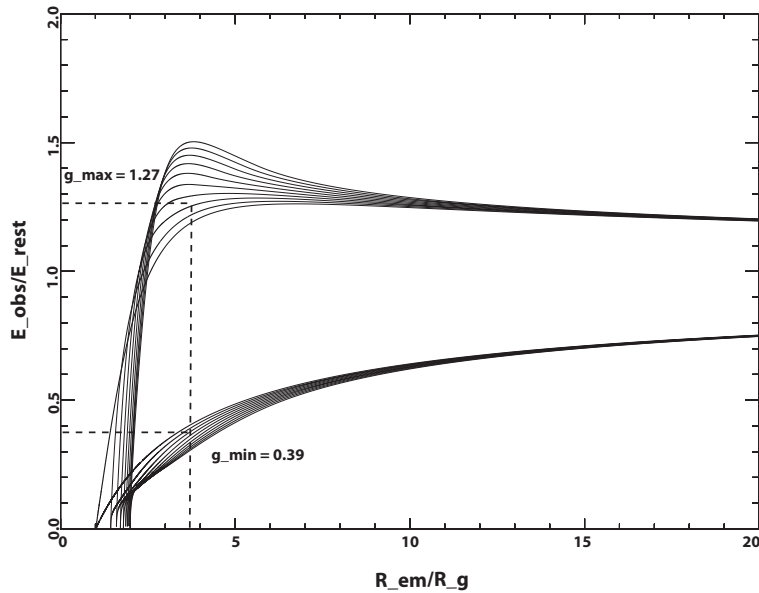
$$g_{\min} = 0.59$$

Assume g_{\min} and g_{\max}
occur at same radius

$$i > 76^\circ$$

$$r_{\text{ISCO}} < 8r_g$$

g versus radius for HE0435



Extremal shifts of the Fe $K\alpha$ line energy in HE 0435 imply $3r_g < r_{\text{ISCO}} < 4r_g$

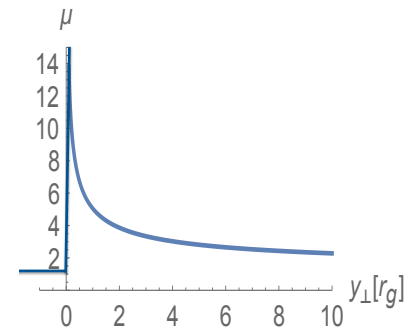
Numerical Simulations of Microlensing Events

(1) Modeling of the Fe-K α emission.

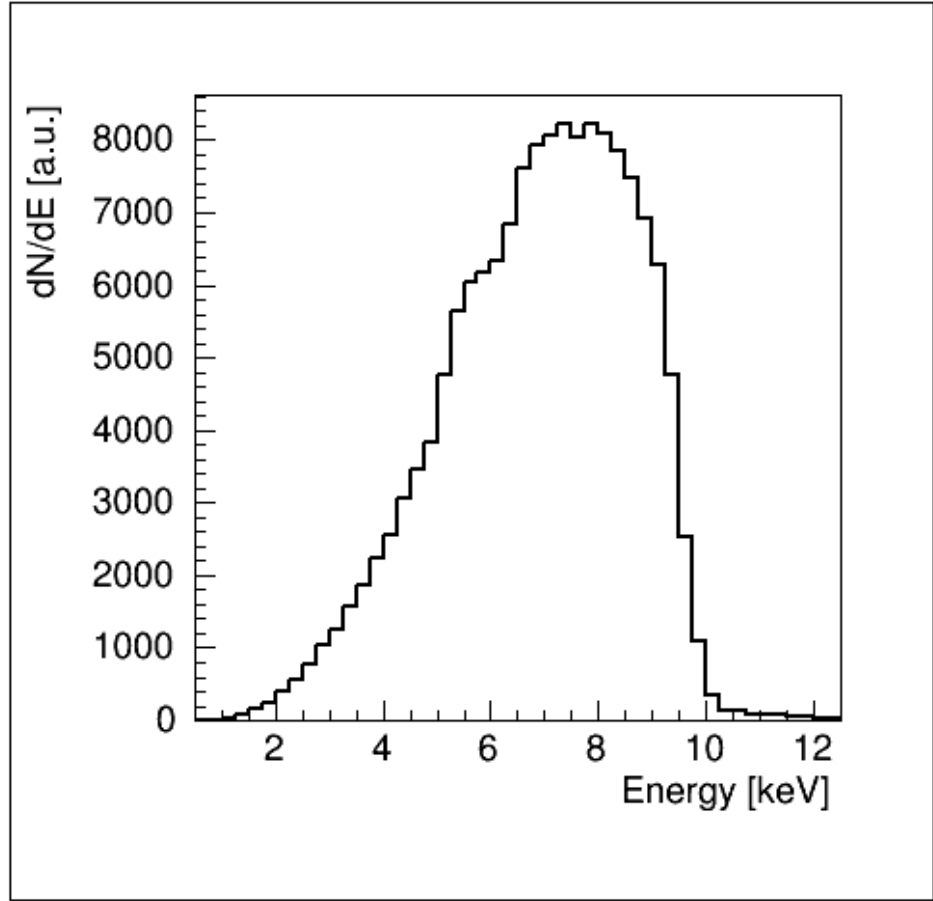
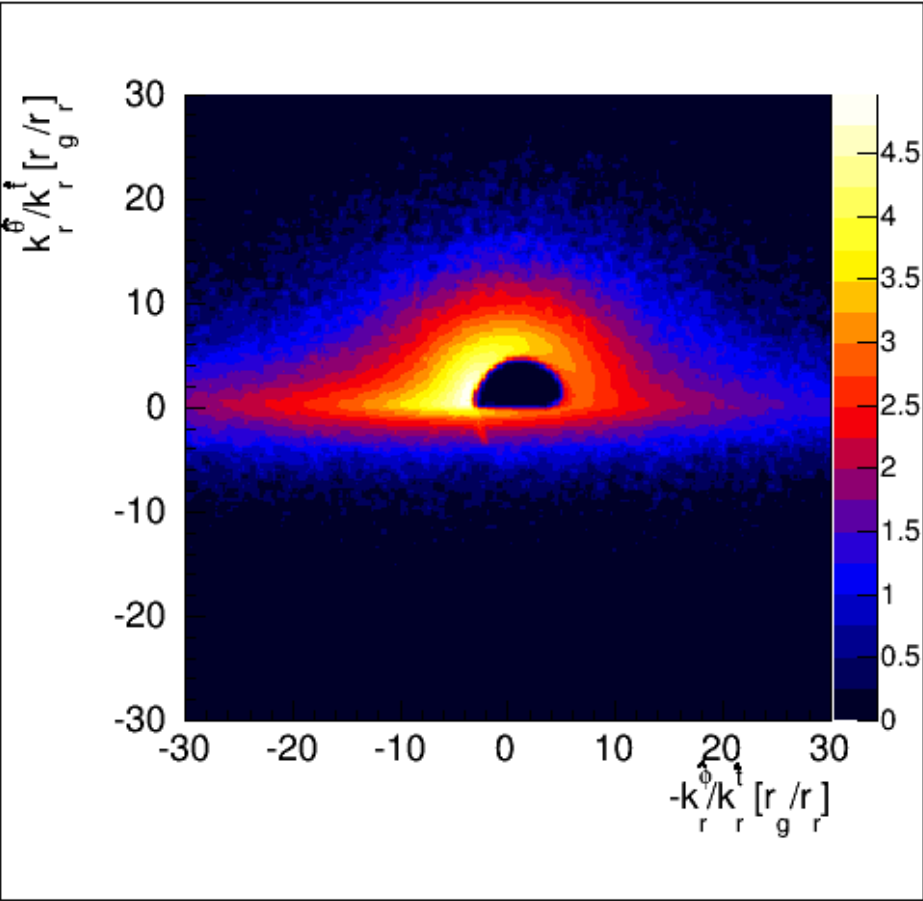
- General relativistic ray tracing code (HK 2012).
- Assume *lamppost*, wedge, or spherical corona.
- Simulate $a=0, 0.1, \dots, 0.9, 0.95, 0.98, 0.998$.

(2) Modeling of Microlensing.

- Inverse ray shooting.
- Simple parameterization of magnification close to caustic fold.

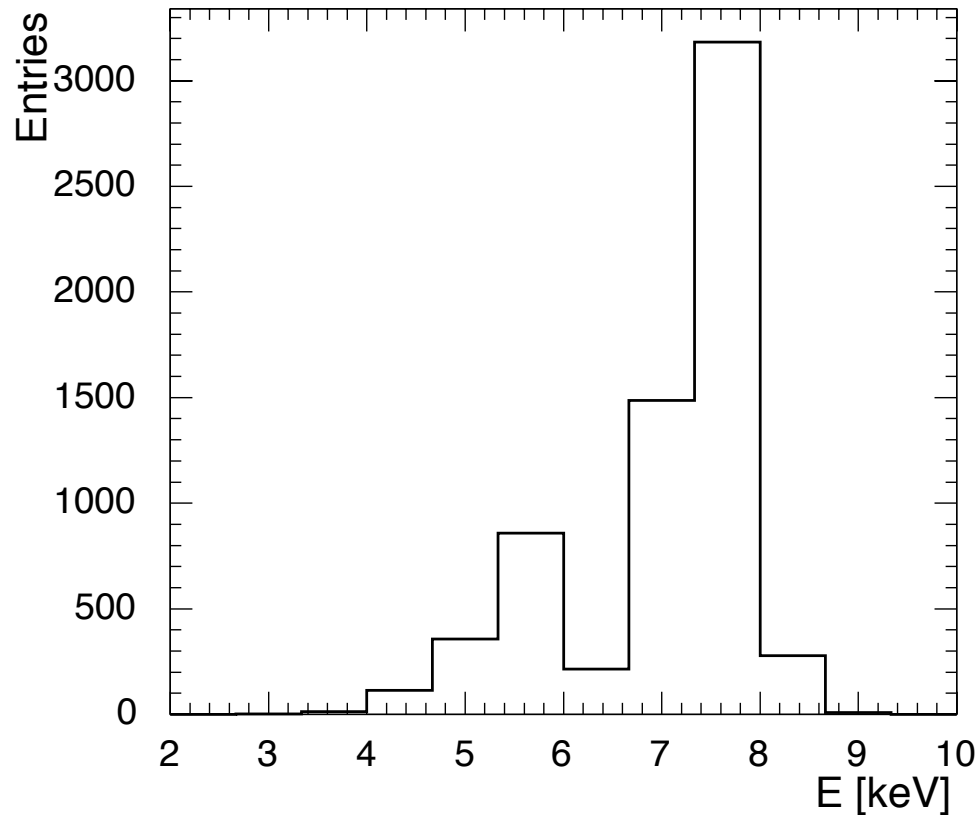


Krawczynski+ 2017



Chartas+ 2016, 2017; Krawczynski+ 2017

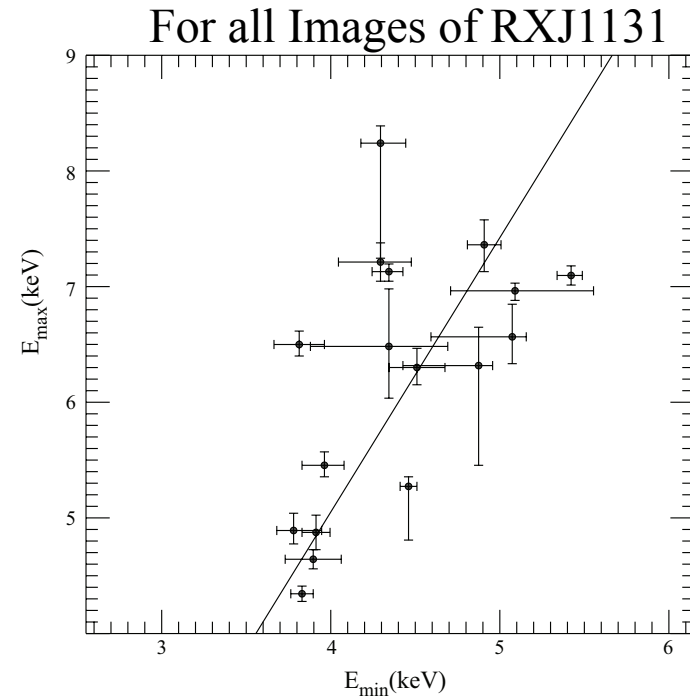
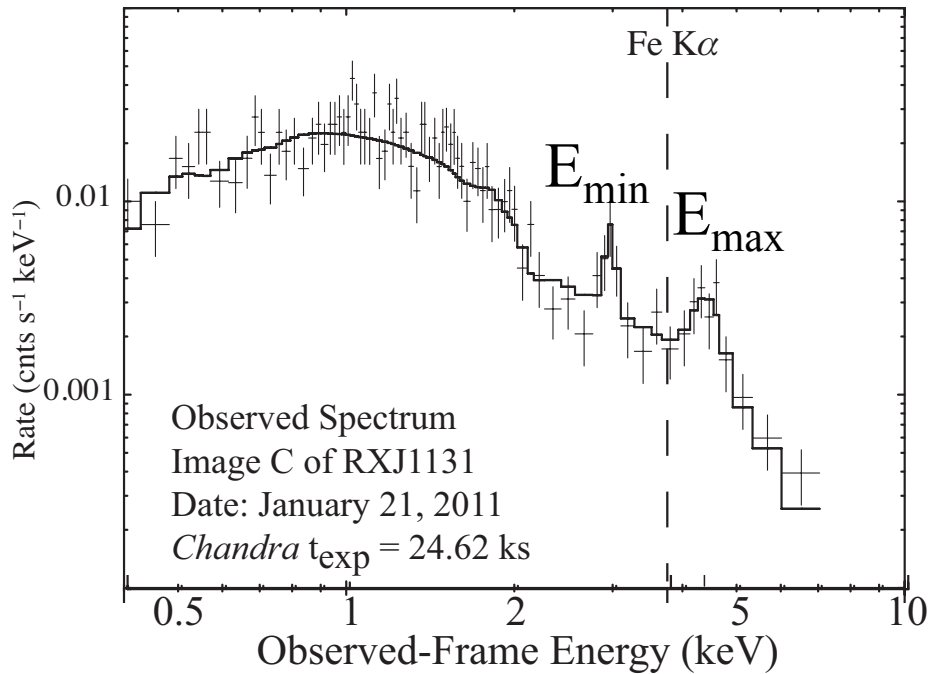
Simulated g-Distribution of Line Centroids



Chartas+ 2016, 2017
Krawczynski+ 2017

Simulated distribution of the single and double peak energies for a black hole with a spin of $a = 0.3$ seen at an inclination of $i = 82.5^\circ$

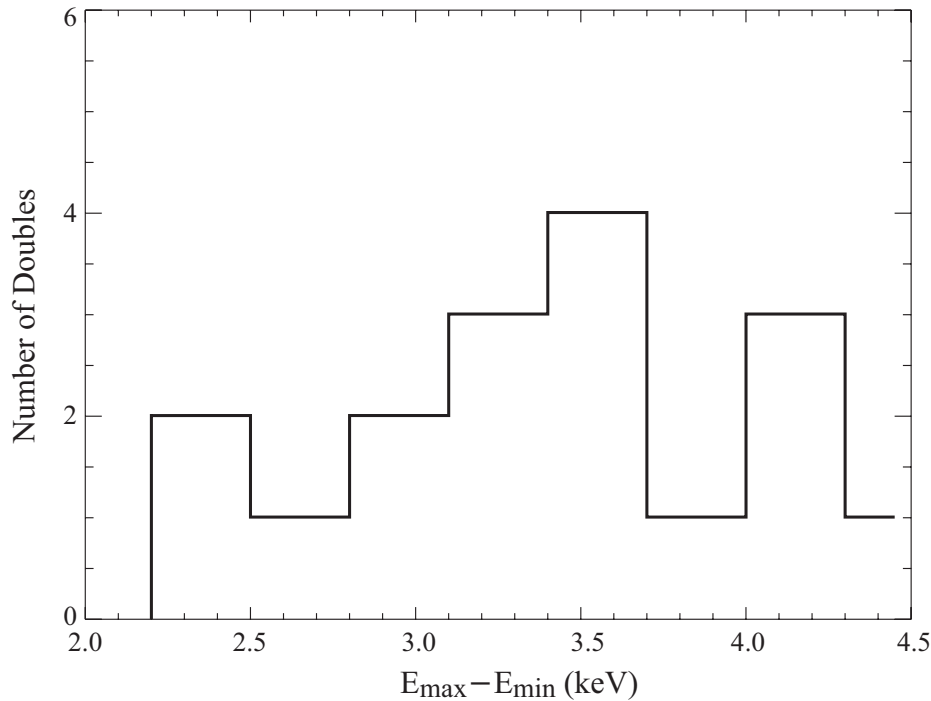
Double Fe $K\alpha$ Emission Lines (“doubles”)



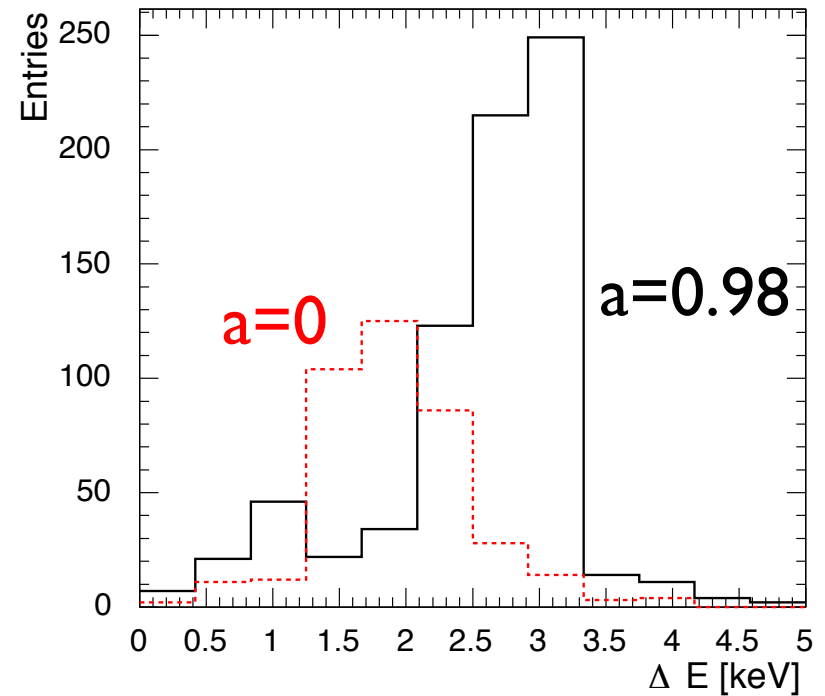
- Double peaks are reproduced in our numerical simulations.
- Moderate correlation between E_{min} and E_{max} :
For image A (Kendall's $\tau = 0.6$, $P > 98\%$ CL)
For all images (Kendall's $\tau = 0.4$, $P > 97\%$ CL)

ΔE -distribution of doubles

Observed ΔE -distribution of RXJ1131



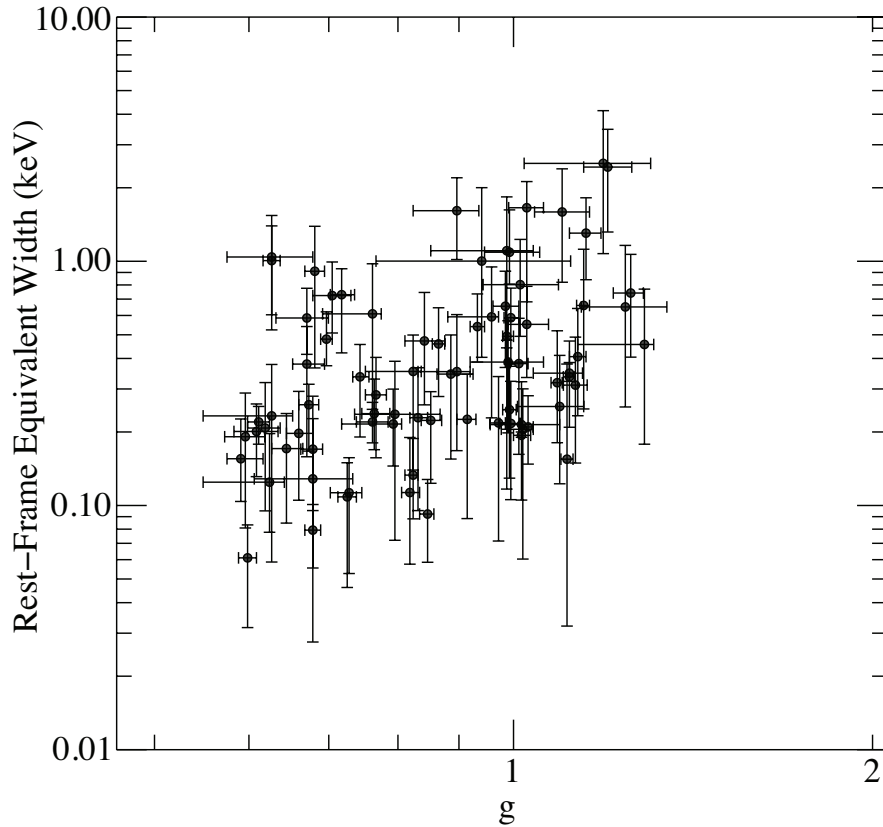
Simulated ΔE -distributions of RXJ1131



Chartas+ 2016, 2017, Krawczynski+ 2017

The distribution of energy separations of doubles depends strongly on black hole spin

g versus Equivalent Width of shifted Fe $K\alpha$ Line



Strong correlation of g vs. EW
Kendall's $\tau = 0.3$, $P > 99.9\%$ CL

One possible explanation of this correlation is that blueshifted line emission is Doppler boosted resulting in the observed EW of the blueshifted lines being larger than the redshifted lines.

Supports microlensing interpretation!

Conclusions

- (1) **Redshifted** and **blueshifted Fe lines** with EWs between 500 – 3000 eV are detected in 5 lensed quasars. We interpret these energy shifts as the **result of microlensing of accretion disk** emission within $\sim 20 r_g$ of the black hole.
- (2) For RXJ1131 we constrain $i > 76^\circ$ and $r_{\text{ISCO}} < 8.5r_g$. For HE 0435 we find $3r_g < r_{\text{ISCO}} < 4r_g$
- (3) Several spectra show two shifted Fe lines (**doubles**). Our numerical simulations reproduce the observable results including the doubles.
- (4) Our simulations show that the distribution of the energy separations of doubles is strongly dependent on spin.
- (5) The next step is to correct for selection bias, fit the results from the numerical simulations to the *Chandra* data and explore the dependence of the results on corona properties.